Lattice dynamics and elastic properties of corundum by the self-consistent atomic deformation method

M. M. Ossowski, L. L. Boyer, and M. J. Mehl
Center for Computational Materials Science, Naval Research Laboratory, Washington, D.C. 20375

H. T. Stokes
Department of Physics and Astronomy, Brigham Young University, Provo, Utah 84602
(Received 17 July 2002; published 12 December 2002)

We apply a recently developed density-functional method based on localized densities to study electronic, structural, elastic, optical, and vibrational properties of α-Al_2O_3. Although our approach is generally less accurate than conventional band-structure methods, calculation of polarization, and related properties is greatly simplified and our results are in reasonably good agreement with experiment and other theoretical calculations. We also assign the symmetry of zone center and other high-symmetry phonon modes and calculate the variation of the zone-center mode frequencies as a function of wave vector direction.

DOI: 10.1103/PhysRevB.66.224302 PACS number(s): 71.15.Mb, 77.22.Ej, 62.20.Dc, 63.20.Dj

I. INTRODUCTION

Corundum (α-Al_2O_3, α-alumina) is one of the most important ceramic materials due its outstanding mechanical and optical characteristics.[1] Because of its high chemical stability corundum finds broad application in a variety of technologies such as radiation detection, thin-film devices, laser manufacturing, catalysis and corrosion, ballistic armor, wear applications and cutting tools, to name just a few. It is also important in high-pressure physics where it is used as a window material for shock-wave experiments, while its Cr^{+3}-doped form (ruby) serves as a pressure calibrant in diamond-anvil cell experiments. The importance of corundum and its metastable polymorphs $\beta, \gamma, \delta, \theta, \kappa$, etc.,[2] is further enhanced by its abundance in the earth's lower mantle where it exists as a high-pressure modification.[3,4]

There has been a steady experimental and theoretical effort to map out the electronic, lattice-dynamical, elastic, optical, etc., properties of corundum. However, the complexity of its crystal structure has hampered the efforts to understand it on a first-principles basis. Only recently, with the increase in computer power, has this begun to change. Following early and limited calculations of the lattice parameters by Salasco *et al.*,[5] who used a linear combination of Gaussian-type orbitals within LDA, Ching and Xu[6] and Mo and Ching[7] applied their method of the self-consistent orthogonalized (frozen-core) linear combination of atomic orbitals, also based on Gaussian-type orbitals and LDA, to study electronic, optical and structural properties of this material. The band widths and various optical properties obtained by them were further refined by Guo *et al.*,[8] using the linearized muffin-tin orbital method in the atomic-sphere approximation, and by Holm *et al.*,[9] using the full-potential linearized muffin-tin orbital method. The last work also included calculation of the elastic properties using the plane-wave pseudopotential method. Elastic properties of corundum were further studied by Boettger[10] who used the high-precision, all-electron, full-potential linear combination of Gaussian type orbitals-fitting function method with considerable success. Recently, lattice-dynamical calculations for corundum were performed by Heid *et al.*[11] by combining the mixed-basis pseudopotential approach with modern density-functional perturbation theory. Finally, very recently, Ouyang and Ching[12] used the finite difference method for the energy gradient in the orthogonalized linear combination of atomic orbitals approach and obtained a high quality Birch fit to the equation of state of corundum.

In the present work we use a recently developed approach based on localized charge densities. In our method the densities are obtained self-consistently by solving one-electron Schrödinger equations, one for each atomic site, whose potentials are determined variationally from the total energy. This is analogous to the Kohn and Sham[13] formulation, the difference being the use of the Thomas-Fermi approximation to the kinetic energy contributions arising from the overlapping charge densities. In accord with Janak's theorem,[14] this variational formulation of potentials automatically minimizes the total energy when the lowest one-electron levels for the entire system are occupied. To solve the Schrödinger equations we use basis functions with radial dependence as listed in tables of Clementi and Roetti[15,16] and angular dependence given by spherical harmonics. This allows the charge densities to relax both radially and nonspherically. We call our method the self-consistent atomic deformation (SCAD) method. SCAD has evolved from Edwardson's[17] attempts to extend the Gordon-Kim[18] electron-gas model to account for nonsphericity of ions. It is formally equivalent to the approach of Cortona[19,20] for spherical ions and closely related to that of Ivanov and Maksimov.[21]

Recently, SCAD has been used to calculate electronic, structural and vibrational properties of number of alkali halides with generally good agreement with experiment. There has been a noted improvement in our calculations over the results obtained from the rigid-ion and related self-consistent atomic models.[22] In addition, SCAD has been applied to calculate polarization and related properties for oxide-based perovskites,[23,24] MgO and AlP.[25] This further confirmed the validity of our model for computing of polarization and re-

lated properties and showed that it can serve as an efficient alternative to the band-structure approach.[26,27]

II. METHOD

In the SCAD method the total electronic charge density of the system is the sum of the overlapped site localized densities

$$n(\mathbf{r}) = \sum_i n_i(\mathbf{r} - \mathbf{R}_i), \tag{1}$$

where the n_i are expanded in terms of spherical harmonics about the sites of the atomic nuclei

$$n_i(\mathbf{r}) = \sum_{l,m} n_{lm}^{(i)}(r) Y_{lm}(\hat{\mathbf{r}}), \tag{2}$$

and the total energy is written

$$E[n(\mathbf{r})] = \sum_i T_0[n_i(\mathbf{r})] + T_k[n(\mathbf{r})] - \sum_i T_k[n_i(\mathbf{r})] + F[n(\mathbf{r})]. \tag{3}$$

Here $T_0[n_i(\mathbf{r})]$ is the kinetic energy of a set of noninteracting electrons centered about the atomic site at $\mathbf{R}_i$ and T_k is a functional which accounts for the kinetic energy due to overlapping densities. Here we use the local Thomas-Fermi expression

$$T_k[n(\mathbf{r})] = \frac{3}{5}(3\pi^2)^{2/3} \int n^{3/5}(\mathbf{r}) d^3r. \tag{4}$$

The remaining functional $F[n(\mathbf{r})]$ contains exchange-correlation[28] and electrostatic contributions to the total energy. Notice that the expression $T_k[n(\mathbf{r})] - \Sigma_i T_k[n_i(\mathbf{r})]$ in Eq. (3) vanishes when the atoms are separated by large distances.

Following a variational procedure similar to that of Kohn and Sham[13] we find that[29] the electrons comprising $n_i(\mathbf{r})$ obey a single-particle Schrödinger equation with potential

$$v_i(\mathbf{r}) = \frac{\delta E[n(\mathbf{r})]}{\delta n_i(\mathbf{r})} = v_F[n(\mathbf{r})] + v_k[n(\mathbf{r})] - v_k[n_i(\mathbf{r})], \tag{5}$$

where

$$v_F[n(\mathbf{r})] = \frac{\delta F[n(\mathbf{r})]}{\delta n(\mathbf{r})} \tag{6}$$

is the functional derivative of $F[n(\mathbf{r})]$ equal to the Kohn-Sham potential and

TABLE I. The seven lowest energy eigenvalues (in Ht) for O and Al in the relaxed $R\bar{3}c$ structure of corundum. The five lowest energy states of Al and five lowest energy states for O are fully occupied.

Ion	1	2	3	4	5	6	7
Al	−55.03	−3.769	−2.399	−2.397	−2.397	0.090	0.090
O	−18.56	−0.815	−0.334	−0.308	−0.269	0.222	0.232

$$v_k[n(\mathbf{r})] = \frac{\delta T_k[n(\mathbf{r})]}{\delta n(\mathbf{r})}. \tag{7}$$

This potential is further expressed in terms of spherical harmonics

$$v_i(\mathbf{r}) = \sum_{l,m} v_{lm}^{(i)}(r) Y_{lm}(\hat{\mathbf{r}}) \tag{8}$$

about the sites of atomic nuclei and the associated one electron Schrödinger equations, one for each atomic site, are solved to obtain new densities $n_i(\mathbf{r})$ and new on-site kinetic energies $T_0[n_i(\mathbf{r})]$. This procedure is then repeated until self-consistency is reached. The one-electron Schrödinger equations are solved using basis functions with radial dependence given by tabulated Slater functions[15,16] and angular dependence given by corresponding spherical harmonics. Additional Y_{lm}'s (up to $l=3$) are included for radial functions of the valence electrons (oxygen p states), resulting in density terms up to $l=6$ (we simply drop those with $l>4$ in the computation of the potential, with negligible error for Al_2O_3). The solution for $v_i(\mathbf{r})$ [and hence, $n_i(\mathbf{r})$ and $n(\mathbf{r})$], obtained by occupying the lowest one-electron energy levels for the entire system, automatically minimizes the total energy in accord with Janak's theorem.[14] These levels, calculated for corundum, are shown in Table I.

The energetics show that the picture of the electronic structure is completely ionic. The valence states of O are fully occupied and 0.36 Ht (1 Ht≃27.2 eV) below the lowest unoccupied states ($3s$) of Al. As a result, no additional charge transfer is required to satisfy the requirements of Janak's theorem. For example, a transfer of 0.05 electrons from the highest occupied level to the lowest unoccupied level gives an increase of 0.1 Ht in the total energy. In other words, the monopole charges are predicted by SCAD to have fixed values, +3 for Al and −2 for O. For comparison with our calculated value of 0.36 Ht, the experimentally determined band gaps are 0.32 Ht (Ref. 30) and 0.36 Ht (Ref. 31). Band structure calculations typically underestimate band gaps values by ~40%. Correspondingly, our value of the gap would be reduced by band broadening. However, one should keep in mind that this value is only an estimate since the Hohenberg-Kohn theorem[32] makes no formal statement about the one-electron states except for the connection between them and the true physical charge density.

In calculating the potentials we divide the space around the atomic site at $\mathbf{R}_i$ into the region inside a sphere of radius

r_c, the ''cutoff'' sphere, where there is a significant charge overlap from the neigboring sites, and the region outside the ''cutoff'' sphere where there is no such significant overlap (r_c is such that the ''cutoff'' sphere typically includes ~ 50 neighbors). Contributions to the potential from the atoms outside the ''cutoff'' sphere are included using Ewald techniques for point monopoles, dipoles and quadrupoles, and directly for $l=3$ and 4. No point-pole approximation is made for contributions to the potential from atoms inside the ''cutoff'' sphere. To handle contributions from atoms inside the ''cutoff'' sphere we extract parts of the potential that are spherically symmetric about $\mathbf{R}_j$ and Löwdin transform[33] them to the corresponding $Y_{l,m}$ expansions about the center at $\mathbf{R}_i$. The $l>0$ contributions, which are relatively smooth near the atomic nuclei at $\mathbf{R}_j$, are computed, together with other smooth parts, on a three-dimensional grid centered at $\mathbf{R}_i$ with a relatively coarse radial mesh and an angular grid chosen for efficient integration.[34] Once the coefficients of the smooth part of the potential are determined by numerical integration they are interpolated from the coarse to the dense radial mesh and combined with the Löwdin transformed and the on-site parts. Finally, the contributions from poles of atoms outside the ''cutoff'' sphere as well as the potential due to the nuclei inside the sphere are added to form the complete representation of the potential for the atom at $\mathbf{R}_i$ in the form given by Eq. (8). A detailed discussion of numerical methods involved in the application of the spherical version of SCAD has been described previously[35] and a comprehensive paper on the general SCAD method is in preparation.[36]

III. CALCULATION OF ELASTIC PROPERTIES

Corundum belongs to the trigonal system, space group $R\bar{3}c$ (D_{3d}^6, No. 167). Its primitive cell is rhombohedral with two formula units. The structure can be viewed as a slightly distorted hexagonal closed-packed lattice of oxygen ions with aluminum ions occupying 2/3 of the octahedral interstices. Each oxygen ion is coordinated with four nearest-neighbor aluminum ions while the aluminum ions are coordinated with six oxygen ions at two different nearest-neighbor distances. Four parameters are needed to describe corundum in this setting: three primitive lattice vectors of equal lengths separated by equal angles and two internal parameters describing the O and Al ions in the $(6e)$ and $(4c)$ positions, respectively. Alternatively, the corundum structure may be regarded as having six formula units in the hexagonal unit cell, where the **c** axis is the threefold axis of the primitive rhombohedral cell, with six layers of closed-packed oxygen ions and with the Al ions located inside the octahedrally coordinated holes.[37] This structure can also be determined by four parameters: the hexagonal lattice constants a and c and two internal positions of the O and Al ions in the $(18e)$ and $(12c)$, respectively. There have been several measurements of the crystal parameters of corundum[38–41] which differ by very little at low temperature. We use the data by Ishizawa *et al.*[41] as the starting point for our calculations. The detailed description of the structure of corundum can be found in an older work by Wyckoff.[38]

TABLE II. Prototypic atomic positions for the relaxed $R\bar{3}c$ structure of corundum. Experimental values (Ref. 41) are given in parentheses.

Prototype	x/a	y/b	c/z	Wyckoff
Al	0	0	0.3552(0.3523)	12(c)
O	0.3067(0.3064)	0	0.25	18(e)

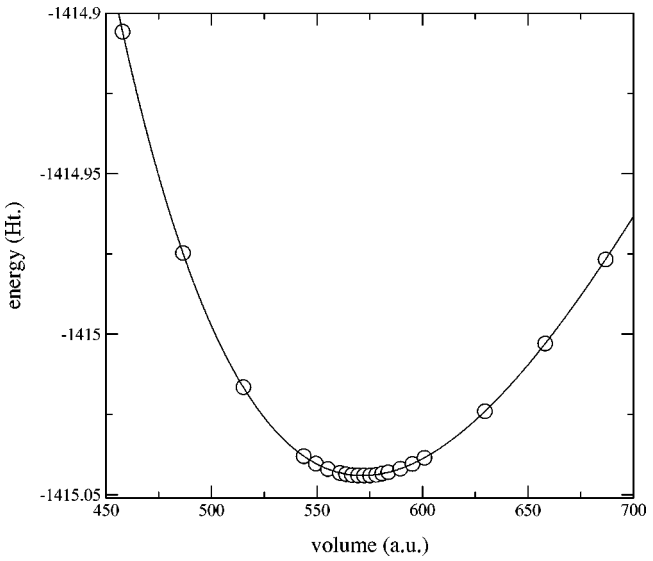

FIG. 1. SCAD total energy values (circles) and four-parameter Birch fit (solid line) for corundum.

We calculate the elastic moduli by applying small strains to the equilibrium lattice, relaxing the structure and calculating the resulting change in the total energy. The equilibrium $R\bar{3}c$ structure is obtained by optimizing each of the four structural parameters independently while the other three are kept constant. The structure is considered at equilibrium when the variation of any of the parameters does not further lower the total energy. The bulk modulus is calculated, as described by Mehl *et al.*,[42] from a four parameter Birch equation[43] fitted to the set of (V_i, E_i) with V_i's within 10% of the equilibrium volume. Fig. 1 shows the quality of our Birch fit and Tables II and III show the calculated values for the equilibrium atomic positions, lattice constants and equilibrium bulk modulus. The comparison with experiment is very good.

In order to calculate the remaining elastic constants we

TABLE III. Lattice constants (in Å), equilibrium bulk modulus (in GPa), and the high-frequency dielectric constant for the relaxed $R\bar{3}c$ structure of corundum.

α-Al_2O_3	a	c	B_0	ϵ_∞^{xx}	ϵ_∞^{zz}
SCAD	4.748	13.02	265	3.5	3.4
Experiment	4.754 [a]	12.99 [a]	267 [b]	3.2 [c]	3.1 [c]

[a]Reference 41.
[b]Reference 44.
[c]Reference 45.

TABLE IV. Strains and elastic moduli for corundum.

Strain	Parameters (unlisted $e_i=0$)	$\Delta E/V$ [to $O(e^2)$]	Space group	V conserving
1	$e_1=e_2=\alpha=(1+\eta)^{-1/3}-1, e_3=\gamma=(1+\eta)^{2/3}-1$	$\frac{1}{9}V[C_{11}+C_{12}+2C_{33}-4C_{13}]\eta^2$	$R\bar{3}c$	yes
2	$e_3=\nu$	$-PV\nu+\frac{1}{2}VC_{33}\nu^2$	$R\bar{3}c$	no
3	$e_1=e_2=\alpha$	$V(C_{11}+C_{12})\alpha^2$	$R\bar{3}c$	no
4	$e_1=\chi$	$-PV\chi+\frac{1}{2}VC_{11}\chi^2$	$C2/c$	no
5	$e_1=\sqrt{\frac{1+\tau}{1-\tau}}-1, e_2=\sqrt{\frac{1-\tau}{1+\tau}}-1$	$(C_{11}-C_{12})\tau^2$	$C2/c$	yes
6	$e_4=\sigma, e_3=\frac{1}{4}\sigma^2$	$\frac{1}{2}VC_{44}\sigma^2$	$C2/c$	yes
7	$e_1=e_4=\eta, e_2=e_3=\mu=\sqrt{1/(1+\eta)+\eta^2/4}-1$	$\frac{1}{2}V(\frac{5}{4}C_{11}-C_{12}+3C_{14}+C_{44})\eta^2$	$C2/c$	yes

write the primitive vectors in the rhombohedral setting and allow the lattice to be strained by some symmetric tensor $\vec{\vec{\varepsilon}}$:

$$\begin{pmatrix}\mathbf{a}_1\\ \mathbf{a}_2\\ \mathbf{a}_3\end{pmatrix}=\begin{pmatrix}+\frac{1}{2}a_h & -\frac{1}{2\sqrt{3}}a_h & \frac{1}{3}c_h\\ 0 & \frac{1}{\sqrt{3}}a_h & \frac{1}{3}c_h\\ -\frac{1}{2}a_h & -\frac{1}{2\sqrt{3}}a_h & \frac{1}{3}c_h\end{pmatrix}\times\begin{pmatrix}1+e_1 & \frac{1}{2}e_6 & \frac{1}{2}e_5\\ \frac{1}{2}e_6 & 1+e_2 & \frac{1}{2}e_4\\ \frac{1}{2}e_5 & \frac{1}{2}e_4 & 1+e_3\end{pmatrix}\begin{pmatrix}\hat{x}\\ \hat{y}\\ \hat{z}\end{pmatrix}, \quad (9)$$

where a_h and c_h are the lattice parameters of the corresponding hexagonal unit cell and where any internal parameters specifying the basis vectors are chosen to minimize the total energy for this lattice. In systems with trigonal symmetry there are six independent elastic constants. Consequently, the total energy can be expressed in terms of the strain variables $\{e_i\}$ as

$$E(\{e_i\})=E_0-P(V)\Delta V+V\sum_{i=1}^{6}\sum_{j=1}^{6}C_{ij}e_ie_j/2+O[\{e_i^3\}]$$

$$=E_0-P(V)\Delta V+V\times\begin{Bmatrix}\frac{1}{2}C_{11}(e_1^2+e_2^2)+C_{12}e_1e_2\\ +\frac{1}{2}C_{33}e_3^2+C_{13}(e_1+e_2)e_3\\ +\frac{1}{2}C_{44}(e_4^2+e_5^2)\\ +C_{14}[(e_1-e_2)e_4+e_5e_6]\\ +\frac{1}{4}(C_{11}-C_{12})e_6^2\end{Bmatrix}+O[\{e_i^3\}], \quad (10)$$

where V is the volume of the undistorted lattice, $P(V)$ is the pressure of the undistorted lattice at volume V, and ΔV is the change in the volume of the lattice due to the strain, Eq. (9). By carefully selecting nonzero strains e_i in Eq. (10) we can directly calculate the corresponding elastic constants or their appropriate linear combinations from the curvature of the least-squares fit of a set of values $(\{e_i\},\Delta E_i)$ to the third order polynomial. We now give a brief description of this procedure.

First, let us consider the strain

$$e_1=e_2=\alpha=(1+\eta)^{-1/3}-1=-\frac{1}{3}\eta+O[\eta^2]$$

and

$$e_3=\gamma=(1+\eta)^{2/3}-1=\frac{2}{3}\eta+O[\eta^2]. \quad (11)$$

This strain is volume conserving, therefore the pressure term in Eq. (9) is zero and we have

$$\Delta E(\eta)=\frac{1}{9}V[C_{11}+C_{12}+2C_{33}-4C_{13}]\eta^2+O[\eta^3], \quad (12)$$

so

$$C_{11}+C_{12}+2C_{33}-4C_{13}=\frac{9}{2V}\Delta E''(0). \quad (13)$$

We can pick a few values of η in the interval [0,0.01], move the atoms within the constraint of the $R\bar{3}c$ symmetry until we find a minimum, and compute $E(\eta)$. The set (η,E) is then least-squares fitted to at least a third order polynomial [to account for the $O[\{\eta^3\}]$ term in Eq. (10)] and the second derivative of $E(\eta)$ is taken at $\eta=0$. In a similar manner we can consider other strains which select out other elastic constants or their linear combinations. These strains are listed in Table IV.

More complicated is the calculation of other elastic constants associated with strains for which the lattice adopts a lower symmetry than the trigonal $R\bar{3}c$. All remaining elastic constants can be calculated from strains which lower the symmetry of the lattice to the space group $C2/c$. Now, however, we have broken the symmetry and it becomes possible for the ions to move to new locations consistent with the

new, lower, symmetry. Therefore, instead of two internal parameters to relax we now have seven. The positions of the atoms in the $C2/c$ space group are listed below. The aluminum atoms are at the $(8f)$ positions

$$\mathbf{b}_1 = +x_1\mathbf{a}_1 + y_1\mathbf{a}_2 + z_1\mathbf{a}_3,$$

$$\mathbf{b}_2 = -z_1\mathbf{a}_1 + \left(\frac{1}{2} - y_1\right)\mathbf{a}_2 - x_1\mathbf{a}_3,$$

$$\mathbf{b}_3 = -x_1\mathbf{a}_1 - y_1\mathbf{a}_2 - z_1\mathbf{a}_3,$$

$$\mathbf{b}_4 = +z_1\mathbf{a}_1 + \left(\frac{1}{2} + y_1\right)\mathbf{a}_2 + x_1\mathbf{a}_3. \quad (14)$$

For the unstrained lattice these reduce to the atomic positions in the $R\bar{3}c$ space group if

$$x_1 = x_{\mathrm{Al}},$$

$$y_1 = x_{\mathrm{Al}},$$

$$z_1 = \frac{1}{2} + x_{\mathrm{Al}}, \quad (15)$$

where x_{Al} is the position of the Al ion at $(4c)$ in the $R\bar{3}c$ space group. Four of the oxygen atoms are also at $(8f)$ positions

$$\mathbf{b}_5 = +x_2\mathbf{a}_1 + y_2\mathbf{a}_2 + z_2\mathbf{a}_3,$$

$$\mathbf{b}_6 = -z_2\mathbf{a}_1 + \left(\frac{1}{2} - y_2\right)\mathbf{a}_2 - x_2\mathbf{a}_3,$$

$$\mathbf{b}_7 = -x_2\mathbf{a}_1 - y_2\mathbf{a}_2 - z_2\mathbf{a}_3,$$

$$\mathbf{b}_8 = +z_2\mathbf{a}_1 + \left(\frac{1}{2} + y_2\right)\mathbf{a}_2 + x_2\mathbf{a}_3. \quad (16)$$

For the unstrained lattice these reduce to the atomic positions in the $R\bar{3}c$ space group if

$$x_2 = x_{\mathrm{O}} - \frac{1}{2},$$

$$y_2 = 1 - x_{\mathrm{O}},$$

$$z_2 = \frac{1}{4}, \quad (17)$$

where x_{O} is the position of the O ion at $(6e)$ in the $R\bar{3}c$ space group. Finally, the two oxygen atoms on the $(4e)$ sites have the coordinates

$$\mathbf{b}_9 = x_3\mathbf{a}_1 + \frac{1}{4}\mathbf{a}_2 + (1 - x_3)\mathbf{a}_3,$$

$$\mathbf{b}_{10} = (1 - x_3)\mathbf{a}_1 + \frac{3}{4}\mathbf{a}_2 + x_3\mathbf{a}_3. \quad (18)$$

TABLE V. Elastic moduli (in GPa) at zero pressure for corundum.

α-Al_2O_3	C_{11}	C_{12}	C_{13}	C_{33}	C_{14}	C_{44}
SCAD	435	167	154	440	−24	86
Experiment[a]	497	164	111	498	−24	147

[a]Reference 44.

Again, for the unstrained lattice $x_3 = x_{\mathrm{O}}$ restores the $R\bar{3}c$ space group symmetry. The rest of the procedure is analogous to the case of the $R\bar{3}c$ symmetry. Notice that not all the strains listed in Table IV are volume conserving. This, however, does not constitute a problem since in these cases the volume change is either linear in the strain (the elastic constants involve only second derivatives) or we ensure that the unstrained cell is at the global equilibrium volume V_0 where $P = 0$. Table V shows the results for calculated elastic constants and compares them with experiment.

The comparison is good with the exception of elastic constants C_{13} and C_{44} which are 30% larger and 40% smaller, respectively, than the experimental values. The all-electron, full potential linear combinations of Gaussian-type orbitals-fitting function method[10] calculations show generally good agreement for elastic constants and, surprisingly, a relatively simple potential induced breathing method (based on spherical ions) also gives good agreement with experiment.[46]

IV. POLARIZATION AND LATTICE DYNAMICS

A convenient feature of SCAD is its relatively straightforward expression of polarization.[25,47] In a band-structure approach, where the charge densities are expressed in terms of functions that are extended throughout the crystal, the attempt to calculate polarization in a unit cell leads to an ambiguity arising from the presence of the term related to the charge that may flow from one unit cell to another. This term,

TABLE VI. Calculated and symmetrized Born effective charges Z_i^* for corundum. The third set contains the *screened* values $\mathbf{Z}_i^*/\sqrt{\epsilon_\infty^{zz}}$ as calculated by Heid, *et al.* (Ref. 11).

	Al			O		
	x	y	z	x	y	z
			Unsymmetrized			
x	3.424	0.060	−0.004	−2.414	0.000	0.000
y	−0.063	3.417	0.001	−0.002	−2.149	0.512
z	0.000	0.000	3.392	0.000	0.485	−2.260
			Symmetrized			
x	3.420	0.061	0.000	−2.411	0.000	0.000
y	−0.061	3.420	0.000	0.000	−2.149	0.515
z	0.000	0.000	3.391	0.000	0.484	−2.264
			Heid *et al.*			
x	1.65	0	0	−1.15	0	0
y	0	1.65	0	0	−1.04	−0.14
z	0	0	1.63	0	−0.19	−1.09

TABLE VII. Calculated zone-center phonon frequencies (in cm^{-1}) for corundum. The compatibility relations as well as the correspondence to the conventional notation are shown. The modes having longitudinal components are labeled as LO. The values from Heid *et al.* (Ref. 11) are given in parentheses.

Mode	1	2	3	4	5
$\Gamma_1^+(A_{1g}):\Lambda_1;\Sigma_1$	337(412)	589(636)			
$\Gamma_2^+(A_{2g}):\Lambda_2;\Sigma_2$	240(301)	510(535)	788(748)		
$\Gamma_3^+(E_g)$(2-fold):$\Lambda_3;\Sigma_1\Sigma_2$	301(377)	327(429)	392(442)	537(568)	698(747)
$\Gamma_1^-(A_{1u}):\Lambda_2;\Sigma_1$	557(594)	683(688)			
$\Gamma_2^-(A_{2u})(\Gamma\mathrm{T}):\Lambda_1$	0(0)	521(500)LO	880(860)LO		
$\Gamma_3^-(E_u)$(2-fold)(ΓT):Λ_3	0(0)	266(382)	362(435)	473(565)	561(628)
$\Gamma_2^-(A_{2u}),\Gamma_3^-(E_u)(\Gamma\mathrm{L})$: $\Sigma_1\Sigma_2$	$0(0)\Sigma_1$	$0(0)\Sigma_2$	$0(0)\Sigma_2$	$266(382)\Sigma_1$	$270(383)\mathrm{LO}\Sigma_2$
	$309(396)\mathrm{LO}\Sigma_2$	$362(435)\Sigma_1$	$410(482)\mathrm{LO}\Sigma_2$	$473(565)\Sigma_1$	$553(625)\mathrm{LO}\Sigma_2$
	$561(571)\Sigma_2$	$561(628)\Sigma_1$	$903(885)\mathrm{LO}\Sigma_2$		
$\Gamma_2^-(A_{2u}),\Gamma_3^-(E_u)(\Gamma\mathrm{F})$: $\Sigma_1\Sigma_2$	$0(0)\Sigma_1$	$0(0)\Sigma_2$	$0(0)\Sigma_2$	$266(382)\Sigma_1$	$268(382)\mathrm{LO}\Sigma_2$
	$326(406)\mathrm{LO}\Sigma_2$	$362(435)\Sigma_1$	$416(484)\mathrm{LO}\Sigma_2$	$473(565)\Sigma_1$	$550(626)\mathrm{LO}\Sigma_2$
	$561(571)\Sigma_2$	$561(628)\Sigma_1$	$899(880)\mathrm{LO}\Sigma_2$		

in general, may depend on the particular choice of the unit cell boundaries and, consequently, the volume integral over $\mathbf{r}\rho(\mathbf{r})$ is ill defined.[48] This problem is solved by expressing changes in polarization ($\mathbf{P}$ itself depends, even in the thermodynamic limit, on the structure of the surface) in terms of currents flowing through the interior of a crystal.[26,27] The resulting Berry's phase approach[49,50] involves computation of difficult integrals over the phases of electronic wave functions. In SCAD, computation of polarization is relatively simple. First, the total charge density is represented as a sum over localized charge densities and, unlike in the band-structure methods, each charge density can be associated with a given ion site. Second, moments of charge are determined by integrations *over all space*. This eliminates the problem of accounting for the surface polarization charges arising when one attempts to compute the dipole moment of a unit cell by integrating *over a finite volume*. In SCAD we calculate the change in the dipole moment $\Delta\mathbf{p}_i$ in terms of the displacement of the monopole charges and the change in the dipole moments of the ions in a structural unit of a crystal.[58] A structural unit, for example, is specified by the space group and occupied Wyckoff positions while the volume V of a structural unit is given by the determinant of the matrix of primitive lattice vectors. Thus, following the definition of polarization as the dipole moment per unit volume we have

$$\Delta\mathbf{P}=\frac{1}{V}\sum_i \Delta\mathbf{p}_i . \tag{19}$$

The change of polarization obtained in this manner is well defined[47] as long as there is no charge transfer from one ion to another. This is certainly the case for Al_2O_3 as we showed in our discussion of the energy eigenstates in Sec. II.

The high-frequency dielectric constant (ϵ_∞) is determined by including additional terms in the $l=1$ parts of the potential. For example, if E_z is the electric field strength in the z direction, then the term $E_z r\sqrt{4\pi/3}$ is added to $v_{1,0}^{(i)}(r)$. In this case the total macroscopic field is just the external field, and the third (z) column of the dielectric tensor is $4\pi P_x/E_z$, $4\pi P_y/E_z$, and $1+4\pi P_z/E_z$, where polarization $\mathbf{P}$ is determined simply by adding the dipole moments induced on each ion in the structural unit divided by the volume of that unit. In principle, the $l=0$ contribution could be included for long wavelength or slab calculations. However, such contributions were shown to be unimportant for MgO, NaCl, and AlP, as was clearly demonstrated by the continuity of the results for

TABLE VIII. Calculated phonon frequencies (in cm^{-1}) for the $T(Z)$, $L(A)$, and $F(D)$ high-symmetry points in corundum. The values from Heid *et al.* (Ref. 11) are given in parentheses.

Mode	1	2	3	4	5	6	7	8	9	10
T_1(4-fold):Λ_3	143(224)	336(424)	423(505)	472(531)	622(692)					
T_3(2-fold):Λ_1,Λ_2	267(324)	359(396)	520(531)	654(659)	845(825)					
L_1(2-fold):none	152(231)	195(246)	218(311)	295(374)	319(404)	380(440)	392(456)	427(497)	436(518)	477(536)
	500(580)	559(625)	600(654)	739(749)	824(818)					
$F_1^+:\Sigma_1$	228(259)	287(353)	363(435)	464(535)	529(559)	627(656)	762(705)			
$F_2^+:\Sigma_2$	108(222)	222(279)	293(364)	329(434)	411(481)	449(546)	544(623)	747(803)		
$F_1^-:\Sigma_1$	260(330)	305(365)	362(394)	387(447)	568(620)	659(657)	805(746)			
$F_2^-:\Sigma_2$	240(305)	266(347)	300(382)	373(468)	443(496)	485(604)	581(755)	732(760)		

phonon dispersion curves near the Γ point.[25] We show our values for ϵ_∞^{xx} and ϵ_∞^{zz} in Table III and compare them with experiment.

In insulators, the nonanalytic contribution to the dynamical matrix, which determines the phonon frequencies at the zone center, is expressed through the high-frequency dielectric constant ϵ_∞ and the Born effective charge tensor Z_i^* (Ref. 51)

$$D_{i\alpha,j\beta}^{\mathrm{LO}} = D_{i\alpha,j\beta}^{\mathrm{TO}} + \frac{4\pi e^2}{V} \frac{(\mathbf{Z}_i^* \cdot \mathbf{q})_\alpha (\mathbf{Z}_j^* \cdot \mathbf{q})_\beta}{\mathbf{q} \cdot \epsilon_\infty \cdot \mathbf{q}}, \tag{20}$$

where Z_i^* is defined as

$$Z_{i;\alpha,\beta}^* = V \frac{\partial P_\alpha}{\partial R_{i;\beta}}, \tag{21}$$

where, $R_{i;\beta}$ is the coordinate of ion i in direction β. As with ϵ_∞, it is relatively easy to calculate Z_i^* within SCAD. We use the fact that SCAD gives a completely ionic picture for the electronic structure of Al_2O_3 with monopole charges which do not vary for small displacements $\delta R_{i;\beta}$ of the ions. Consequently, the Born effective charges can be computed as

$$Z_{i;\alpha,\beta}^* = Z_i \delta_{\alpha\beta} + \sum_j \frac{\partial p_{j;\alpha}}{\partial R_{i;\beta}}, \tag{22}$$

where Z_i are the monopoles and $\mathbf{p}_j$ are the dipole moments calculated self-consistently by SCAD for each displacement $\mathbf{R}_i$.

We calculate tensors Z_i^* separately for *all* ions in the unit cell and rotate them into symmetrically equivalent sites averaging the results obtained for each site. This way we ensure that the small numerical uncertainties due to the direction-dependent choice of the angular integration mesh used in our calculation of the potentials are averaged out. Table VI illustrates this procedure by showing the ''raw'' and symmetrized Born effective charge tensors. To compare our Z_i^* values with those obtained from a mixed-basis pseudopotential approach and LDA (Ref. 11) our values need to be divided by $\sqrt{\epsilon_\infty^{zz}}$. While the off-diagonal elements in the Born effective charge tensors calculated by us remain small, they are markedly larger than reported by Heid *et al.*,[11] especially for oxygen. For all the elements the sum rule in our calculation is satisfied to better than 0.02.

Vibrational frequencies are calculated using a symmetrized frozen phonon technique.[52,59] First, sets of orthogonal frozen modes are determined for each irreducible representation (IR). The number of modes in a set for a given IR is the number of nonzero frequencies divided by their degeneracy. Next, the energy as a function of displacement amplitude is calculated for each mode and their pairwise linear combinations. The curvature of these energy functions at zero amplitude gives the elements of the block diagonalized analytical part of the dynamical matrix D, Eq. (20). We supply the elements of D by calculating curvatures of parabolas from changes in energy for small displacements consistent with each frozen mode. In fact, to improve the accuracy, these calculations are carried out twice, the second pass using the projected modes with amplitudes consistent with eigenvectors obtained in the first pass.

In the following we use the notation of Miller and Love,[53] adopted by Stokes and Hatch,[54] and show the corresponding Koster[55] and conventional labels in Tables VII and VIII, for easy comparison with literature. In this paper we consider the high-symmetry points Γ, L, F, and T. In $R\bar{3}c$, at Γ we have two Γ_1^+ modes, three Γ_2^+ modes, two Γ_1^- modes, three (counting the 0 frequency translational mode) Γ_2^- modes, five doubly degenerate Γ_3^+, modes and five (counting the 0 frequency translational mode) doubly degenerate Γ_3^- modes. The Γ_3^- degeneracy is removed at $\mathbf{k} \approx 0$ in directions other than that of the crystallographic axis **c**. This effect, which is included in the nonanalytic term of the dynamical matrix D, Eq. (20), is due to long-range macroscopic polarization fields that affect the modes with a LO component. The LO-TO splitting for the Γ_3^- modes is the largest in the plane perpendicular to the **c** axis. On the other hand, the Γ_2^- modes are purely transverse in this plane and purely longitudinal in the **c** direction. The modes belonging to Γ_1^+, Γ_2^+, Γ_3^+ and Γ_1^- are not polar modes and thus are not affected by the nonanalytic term in Eq. (20).

We show the calculated frequencies for the Γ point in Table VII and for the T, L, and F points (ΓL and ΓF directions are *not* in the plane perpendicular to the ΓZ direction—the direction of the **c** axis.) in Table VIII. Our results are compared with the results from the density-functional perturbation theory calculations,[11] which agree remarkably well with the experimental data obtained for **k** points along the special lines Λ and Σ.[56]

A comment, however, must be made. For the Γ point we have the following compatibility relations with Σ: $\Gamma_1^+ : \Sigma_1$, $\Gamma_2^+ : \Sigma_2$, $\Gamma_3^+ : \Sigma_1 \Sigma_2$, $\Gamma_1^- : \Sigma_1$, $\Gamma_2^- : \Sigma_2$, $\Gamma_3^- : \Sigma_1 \Sigma_2$. For F the compatibility relations with Σ are $F_1^+ : \Sigma_1$, $F_2^+ : \Sigma_2$, $F_1^- : \Sigma_1$,

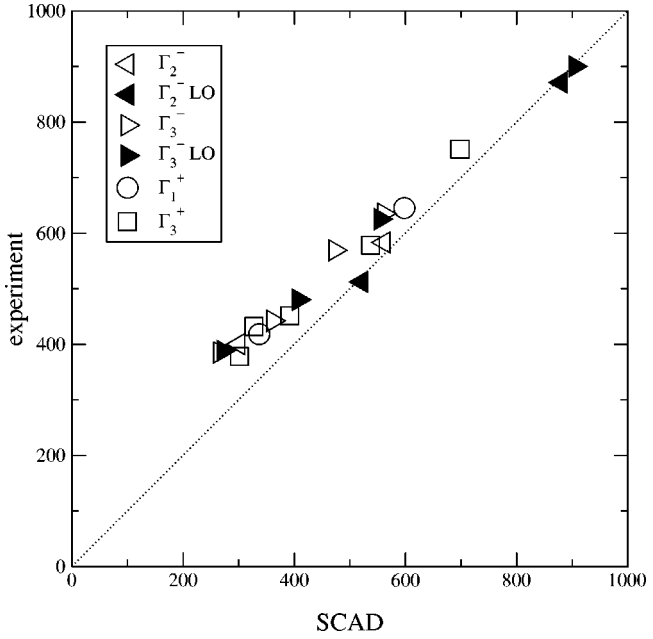

FIG. 2. Calculated vs experimental (Refs. 45 and 57) zone center phonon frequencies (in cm^{-1}) for corundum.

$F_2^-:\Sigma_2$. Counting modes at Γ we obtain $2\Gamma_1^+ \rightarrow 2\Sigma_1$, $3\Gamma_2^+ \rightarrow 3\Sigma_2$, $10\Gamma_3^+ \rightarrow 5\Sigma_1 + 5\Sigma_2$, $2\Gamma_1^- \rightarrow 2\Sigma_1$, $3\Gamma_2^- \rightarrow 3\Sigma_2$, $10\Gamma_3^- \rightarrow 5\Sigma_1 + 5\Sigma_2$. This results in 14 Σ_1 modes and 16 Σ_2, consistent with the F point where we have 7 F_1^+ modes, 8 F_2^+ modes, 7 F_1^- modes and 8 F_2^+ modes. The authors of the cited theoretical[11] and experimental[56] papers appear to have mislabeled their Σ_1 and Σ_2 modes, effectively connecting Γ_2^- and Γ_3^- LO modes to Σ_1 and Γ_1^- and Γ_3^- TO modes to Σ_1, for both ΓL and ΓF directions. This led to an incorrect assignment of 15 modes to Σ_1 and 15 modes to Σ_2. Consequently, their labels at F are also incorrect. Using the authors' own assignments for the infrared-active and Raman-active and silent modes,[11] which are correct, we were able to properly relabel their Σ_1 and Σ_2 modes. This new assignment is reflected in Tables VII and VIII.

To compare our results with the experimental infrared and Raman data we did additional calculations for the Γ_3^- frequencies at $\mathbf{k} \approx 0$ in the plane perpendicular to $\mathbf{c}$. These frequencies can be directly compared with the experimental values for the infrared-active E_u LO modes. The infrared-active A_{2u} LO frequencies have already been calculated as the Γ_2^- frequencies for $\mathbf{k} \approx 0$ in the ΓZ direction. The frequencies of all the infrared-active TO and Raman-active modes have been determined by diagonalizing the dynamical matrix D, Eq. (20) without the macroscopic field term. These results are shown in Fig. 2.

V. SUMMARY

We illustrate the SCAD method for calculating polarization and related properties for the nontrivial case of corundum. The results which we obtain for phonon frequencies are in reasonably good agreement with experiment (we have an average error of 14% and slightly larger error for the low-frequency modes in Fig. 2 and Tables VII and VIII). We find excellent agreement for the structural parameters and most of the elastic constants (with the exception of C_{13} and C_{44}).

ACKNOWLEDGMENTS

This work was supported by the National Research Council and the Office of Naval Research. We are grateful to Dr. J. L. Feldman and Dr. A. G. Petukhov for helpful discussions.

[1] E. Dörre and H. Hübner, *Alumina* (Springer-Verlag, Berlin, 1984).
[2] I. Levin and D. Brandon, J. Am. Ceram. Soc. **81**, 1995 (1998).
[3] W. Duan, R.M. Wentzcovitch, and K.T. Thomson, Phys. Rev. B **57**, 10 363 (1998).
[4] F.C. Marton and R.E. Cohen, Am. Mineral. **79**, 789 (1994).
[5] L. Salasco, R. Dovesi, R. Orlando, M. Causa, and V.R. Saunders, Mol. Phys. **72**, 267 (1991).
[6] W.Y. Ching and Y.N. Xu, J. Am. Ceram. Soc. **77**, 404 (1994).
[7] S.D. Mo and W.Y. Ching, Phys. Rev. B **57**, 15 219 (1998).
[8] X. Guo, S. Canney, A.S. Kheifets, M. Vos, Z. Fang, S. Utteridge, I.E. McCarthy, and E. Weigold, Phys. Rev. B **54**, 17 943 (1996).
[9] B. Holm, R. Ahuja, B. Johansson, and B.I. Lundqvist, Phys. Rev. B **59**, 12 777 (1999).
[10] J.C. Boettger, Phys. Rev. B **55**, 750 (1997).
[11] R. Heid, D. Strauch, and K.P. Bohnen, Phys. Rev. B **61**, 8625 (2000); R. Heid (private communication).
[12] L. Ouyang and W.Y. Ching, J. Am. Ceram. Soc. **84**, 801 (2001).
[13] W. Kohn and L.J. Sham, Phys. Rev. **140**, A1133 (1965).
[14] J.F. Janak, Phys. Rev. B **18**, 7165 (1978).
[15] E. Clementi and C. Roetti, At. Data Nucl. Data Tables **14**, 177 (1974).
[16] A.D. McLean and R.S. McLean, At. Data Nucl. Data Tables **26**, 197 (1981).
[17] P.J. Edwardson, Phys. Rev. Lett. **63**, 55 (1989).
[18] R.G. Gordon and Y.S. Kim, J. Chem. Phys. **56**, 3122 (1972).
[19] P. Cortona, Phys. Rev. B **44**, 8454 (1991).
[20] P. Cortona, Phys. Rev. B **46**, 2208 (1992).
[21] O.V. Ivanov and E.G. Maksimov, Phys. Rev. Lett. **69**, 108 (1992); Solid State Commun. **97**, 163 (1996).
[22] W.N. Mei, L.L. Boyer, M.J. Mehl, M.M. Ossowski, and H.T. Stokes, Phys. Rev. B **61**, 11 425 (2000).
[23] L.L. Boyer, H.T. Stokes, and M.J. Mehl, Ferroelectrics **194**, 173 (1997).
[24] L.L. Boyer, H.T. Stokes, and M.J. Mehl, in *First Principles Calculations for Ferroelectrics*, edited by R. E. Cohen, AIP Conf. Proc. No. 436 (AIP, Melville, 1998), p. 227.
[25] L.L. Boyer, H.T. Stokes, and M.J. Mehl, Phys. Rev. Lett. **84**, 709 (2000).
[26] R.D. King-Smith and D. Vanderbilt, Phys. Rev. B **47**, 1651 (1993).
[27] R. Resta, Rev. Mod. Phys. **66**, 899 (1994).
[28] L. Hedin and B.I. Lundqvist, J. Phys. C **4**, 2064 (1971).
[29] M.J. Mehl, H.T. Stokes, and L.L. Boyer, J. Phys. Chem. Solids **57**, 1405 (1996).
[30] M.L. Bortz, R.H. French, D.J. Jones, R.V. Kasowski, and S. Obuchi, Phys. Scr. **41**, 4404 (1990); M.L. Bortz and R.H. French, Appl. Phys. Lett. **55**, 1955 (1989).
[31] E.T. Arakawa and M.W. Williams, J. Phys. Chem. Solids **29**, 735 (1968).
[32] P. Hohenberg and W. Kohn, Phys. Rev. **136**, B864 (1964).
[33] G.C. Fletcher, *The Electron Band Theory of Solids* (North Holland/Amsterdam, 1971).
[34] D.C. Patton, D.V. Porezag, and M.R. Pederson, Phys. Rev. B **55**, 7454 (1997).
[35] H.T. Stokes, L.L. Boyer, and M.J. Mehl, Phys. Rev. B **54**, 7729 (1996).
[36] L.L. Boyer, H.T. Stokes, M.J. Mehl, and M.M. Ossowski (unpublished).
[37] F.S. Galasso, *Structure and Properties of Inorganic Solids* (Pergamon, New York, 1970).
[38] R.W.G. Wyckoff, *Crystal Structures* (Wiley, New York, 1964).
[39] J. Lewis, D. Schwarzenbach, and H.D. Flack, Acta Crystallogr., Sect. A: Found. Crystallogr. **38**, 733 (1982).

[40] P. Aldebert and J.P. Traverse, J. Am. Ceram. Soc. **65**, 460 (1982).
[41] N. Ishizawa, T. Miyata, I. Minato, F. Marumo, and S. Iwai, Acta Crystallogr., Sect. B: Struct. Crystallogr. Cryst. Chem. **36**, 228 (1980).
[42] M.J. Mehl, B.M. Klein, and D.A. Papaconstantopoulos, in *Intermetallic Compounds—Principles and Practice*, edited by J.H. Westbrook and R.L. Fleischer (Wiley, London, 1994), Vol. 1, p. 195.
[43] F. Birch, J. Geophys. Res. **83**, 1257 (1978).
[44] J.B. Watchman, Jr., W.E. Teft, D.G. Lam, Jr., and R.P. Stinchfield, J. Res. Natl. Bur. Stand. **64**, 213 (1960).
[45] A.S. Barker, Jr., Phys. Rev. **132**, 1474 (1963).
[46] R.E. Cohen, Geophys. Res. Lett. **14**, 37 (1987).
[47] L.L. Boyer, M.J. Mehl, and H.T. Stokes, Phys. Rev. B **66**, 092106 (2002).
[48] R.M. Martin, Phys. Rev. B **9**, 1998 (1974).
[49] M.V. Berry, Proc. R. Soc. London, Ser. A **392**, 45 (1984).
[50] R.M. Martin and G. Ortiz, Solid State Commun. **102**, 121 (1997).
[51] P. Giannozi, S. Gironcoli, P. Pavone, and S. Baroni, Phys. Rev. B **43**, 7231 (1991).
[52] H.T. Stokes, Ferroelectrics **164**, 183 (1995).
[53] S.C. Miller and W.F. Love, *Tables of Irreducible Reperesentations of Space Groups and Co-Representations of Magnetic Space Groups* (Pruett, Boulder, 1967).
[54] H.T. Stokes and D.M. Hatch, *Isotropy Subgroups of the 230 Crystallographic Space Groups* (World Scientific, Singapore, 1988).
[55] G.F. Koster, Solid State Phys. **5**, 173 (1957).
[56] H. Schober, D. Strauch, and B. Dorner, Z. Phys. B: Condens. Matter **92**, 273 (1993).
[57] S.P.S. Porto and R.S. Krishnan, J. Chem. Phys. **47**, 1009 (1967).
[58] Here, we use the term ''structural unit'' rather than ''unit cell'' to emphasize that our calculation does not depend on a particular choice of unit cell boundaries.
[59] Symmetry constraints of the frozen-phonon method are imposed automatically using code based on the work by H.T. Stokes and D.M. Hatch, *Isotropy Subgroups of the 230 Crystallographic Space Groups* (World Scientific, Singapore, 1988). The code is available at http://128.187.202.55/~stokesh/isotropy.html